공학석사학위논문

Preparation and Characterization of Porous Carbon Nanotubes for High Rate Capability Li-S Batteries

고성능의 리튬황전지를 위한 다공성 탄소나노튜브들의 제작 및 특성 연구

2014년 8월

서울대학교 대학원

재료공학부

정 요 찬

Preparation and characterization of porous carbon nanotubes for high rate capability Li-S batteries

고성능 리튬-황전지를 위한

다공성 탄소나노튜브의 제작 및 특성 연구

지도 교수 박 종 래

이 논문을 공학석사 학위논문으로 제출함

2014년 7월

서울대학교 대학원

재료공학부

정 요 찬

정요찬의 석사 학위논문을 인준함

2014년 7월

위 원 장 조 원 호 (인)

부위원장 박 종 래 (인)

위 원 장 지 영 (인)

Abstract

Preparation and Characterization of Porous Carbon Nanotubes for High Rate Capability Li-S Battery

Jeong, Yo Chan
Department of Material Science and Engineering
The Graduate School
Seoul National University

Porous carbon nanotubes were prepared through KOH activation and investigated for the application of high performance lithium sulfur batteries. Through KOH activation, enhanced specific surface area for reducing electron penetration depth and increased pore volume for sulfur loading were achieved. In addition, oxygen containing functional groups which are known to interact with polysulfide and lithium sulfide were realized on the carbon matrix.

Electrochemical performances affected by morphological and chemical changes of porous carbon matrix and uniformity of sulfur loaded on carbon nanotubes were examined. Three methods of

preparing CNT/sulfur composites were studied. It was found that uniform distribution of sulfur on the carbon matrix prepared through the solution-based sulfur precipitation method followed by thermal treatment gave the best electrochemical performance.

Porous CNT/sulfur composite which was activated for 2 hours delivered the highest performance of 688 mAh/g at 5 C and retained 672 mAh/g even after 50 cycles. This outstanding performance was proven to be originated from the shorten electron penetration depth and guaranteed lithium ion diffusion pathway in the composite.

keywords : porous carbon nanotubes, carbon nanotubes, lithium sulfur batteries, high rate capability, high performance batteries and cathode materials.

Student Number: 2012-23151

Contents

List of Tables

List of Figures

1 Introduction

1.1 General introduction of lithium sulfur batteries (LSBs)

1.1.1 Increasing demands on the high energy density batteries.

Due to energy crisis and environmental issue, electric vehicles and large scale energy storage systems have captured the great interest among many scientists. Currently commercialized lithium ion batteries have limited energy density, only 387 $Whkg^{-1}$ in the case of $LiCoO_2$/C battery.[1] In the application of portable devices such as laptops, smart-phones, the energy density of lithium ion batteries is acceptable.

However, the energy density of batteries is required to be improved for the application of civil transportation, large scale energy storage systems.[2] Thus, surging demands on high energy density batteries are driving the global research efforts into other types of batteries such as lithium-sulfur batteries and lithium-air batteries with higher theoretical energy density.

1.1.2 Opportunities of LSBs

The first lithium sulfur battery was discovered in the 1960s.[3] The theoretical energy density of lithium sulfur batteries is around 2600 $Whkg^{-1}$ based on the combination of lithium metal anode and sulfur cathode. This value is five times higher than the value of commercialized lithium ion battery.

In addition to the higher energy density of lithium sulfur batteries, the low cost of sulfur is attractive. In fact, the cost of cobalt is very expansive compared to the value of sulfur. Fig. 1 showed the piles of yellow sulfur at a terminal near Vancouver which illustrated the abundance of sulfur, only $105 per ton while cobalt costs around $30,000 per ton which traded in London metal exchange.

Besides, the low operating voltage of 2.15 versus Li/Li+ could improve the safety which has been a great deal of lithium ion batteries.[4] The sudden explosion of lithium ion batteries has not been alleviated since it was commercialized. More than 40 recalls due to explosion risk from lithium ion batteries in portable devices have been reported. Lithium sulfur batteries can alleviate this risk of explosion or fire issue. There merits provide great opportunities for next-generation energy

storage system beyond lithium ion batteries.

1.1.3 Challenges of LSBs

Before discussing the challenges, it is necessary to see what happens when lithium sulfur batteries work. Many researches provided insights into the mechanism.[5-9] Schematic illustration of a proposed sulfur reduction mechanism is shown in Fig. 1. Elemental sulfur (cyclo-S_8) reacts with lithium metal in multistep electrochemical process. In the reaction around 2.4-2.2 V (vs Li+/Li), long polysulfide chains are produced. In the second part around 2.15-2.1 V (vs Li+/Li), long polysulfide chains are further shortened into S_4^{2-}. For the end of this reduction process between 2.1-1.9 V (vs Li+/Li), short polysulfides such as S_3^{2-}, S_2^{2-}, and S^{2-} are produced.[6]

Because lithium sulfur batteries follow multistep reactions, the structural and morphological changes are inevitable. Thus intermediate polysulfides play a critical role in deciding the electrochemical performance.

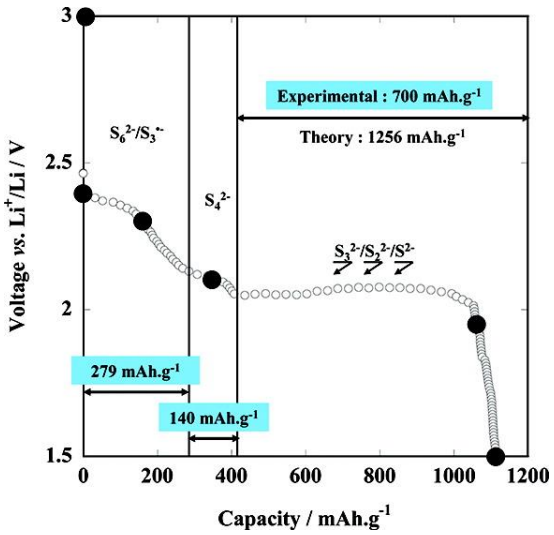

Figure 1 Schematic illustration of a proposed sulfur reduction mechanism[6]

In fact, polysulfides with longer chains (Li_2Sx, $3 \leq x \leq 8$) are soluble in liquid electrolyte and shuttle back and forth between the lithium anode and the cathode leading to side reactions, which were known as 'shuttle phenomenon'.[6] These side reactions lead to the incomplete sulfur active material utilization and drastic capacity fading with cycling.[1]

Insulating nature of sulfur also causes the problem such as low electrochemical utilization and limited rate capability.[2] The remedy for the poor intrinsic conductivity of 5×10^{-30} Scm^{-1} at room temperature

should be provided for the commercialization of lithium sulfur batteries.

In addition, inevitable volume expansion causes damage on cathode even though this issue might not be severe as silicon anode case. These demerits of lithium sulfur batteries should be alleviated in order to be commercialized.

1.2 Current strategies addressing the challenges of LSBs

Several types of strategies have attempted to overcome the hurdles of lithium sulfur batteries. It included the introduction of various carbon materials as a conducting matrix for insulating sulfur, functionalization of introduced carbon materials, insertion of physical barriers and solid electrolytes.

1.2.1 Porous carbon materials

In 2009 , Nazar and coworkers reported the usefulness of highly ordered mesoporous carbon as a conductive matrix for alleviating polysulfide diffusion into bulk electrolyte.[10] After this monumental report, various porous carbon materials including carbide-derived

carbon foam[11], MOF-derived carbon[12], self-assembled colloid-derived carbon[13], crosslinked graphene[14] and graphene wrapped CNF[15] were studied for improved lithium sulfur batteries.

These porous carbon materials were effective in addressing the polysulfide issue, thus, improving the capacity stability as shown in Fig. 2 and Fig. 3.

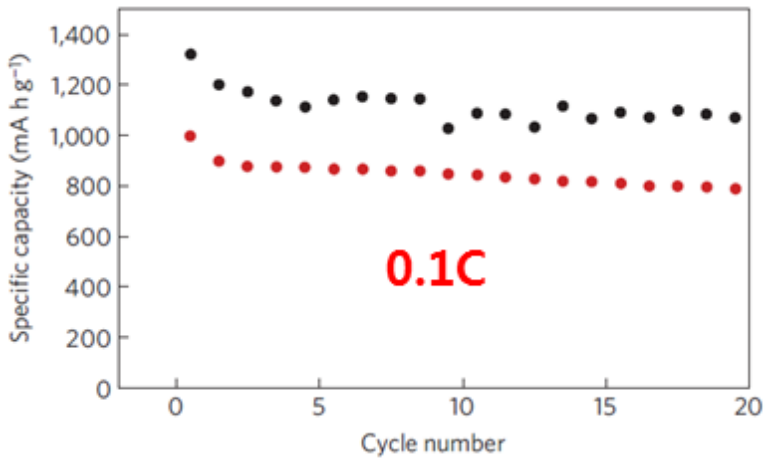

Figure 2 Improved cycle stability with ordered mesoporous carbon[10]

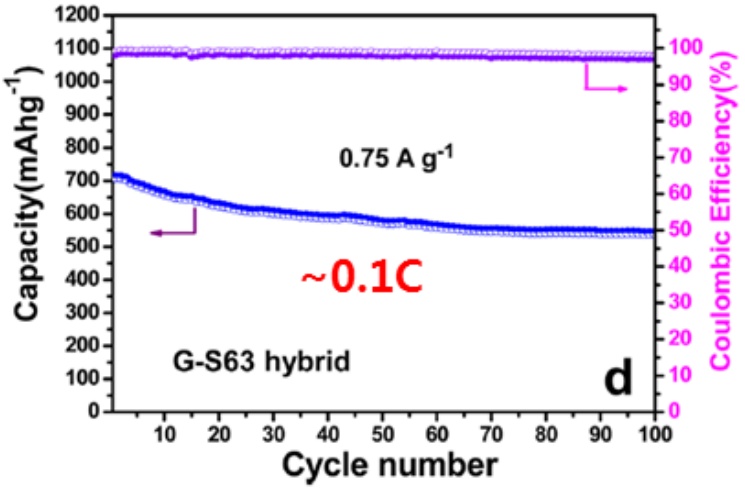

Figure 3 Improved cycle stability with crosslinked graphene[14]

1.2.2 Functionalization on carbon materials

Previously mentioned reports have established the effect of porous carbon matrix in improving cycle stability. For further improvement, functionalization of carbon matrix has currently studied. For one example, amphiphilic surface modification of hollow carbon nanofibers was reported for the purpose of enhancing cycle life as shown in Fig. 4.[16]

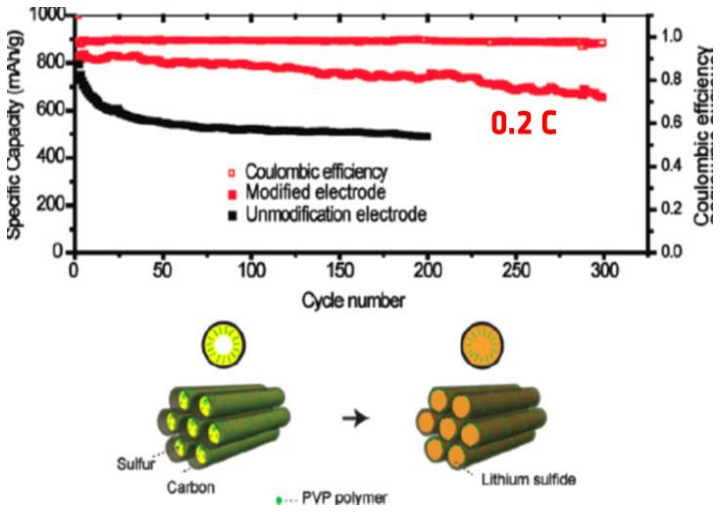

Figure 4 Enhanced cycle life with amphiphilic surface modification of hollow carbon nanofibers[16]

For another example, hydroxylated graphene-sulfur nanocomposite was also reported.[17] This also proved the effect of functionalization on carbon materials.

1.2.3 Insertion of physical barriers

Except focusing on the carbon materials of cathode, configuration change such as insertion of CNT film[18] or graphene sheet[19] between separator and sulfur cathode is attempted to address the challenges. The interlayers seem to play a role as polysulfide reservoir. As presented in Fig. 5, it seems to work at low charge/discharge rate, 0.2 C and 1 C.

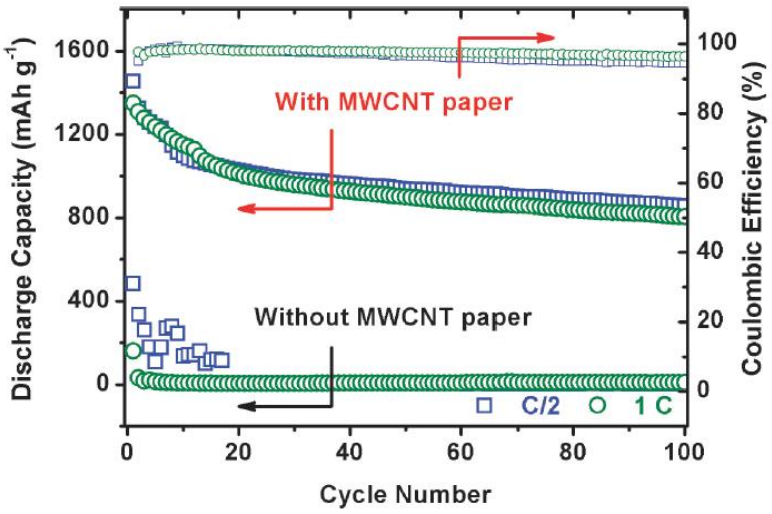

Figure 5 Rate capability and cycle stability of CNT intercalated LSB[18]

1.2.4 Electrolytes

Approaches on electrolyte have been conducted with the recognition of a primary role of electrolyte in that it gives transport path of lithium ion and polysulfide. The effect of concentrated liquid electrolyte has studied.[20] By using solid electrolyte, all-solid-state lithium battery is also currently reported.[21]

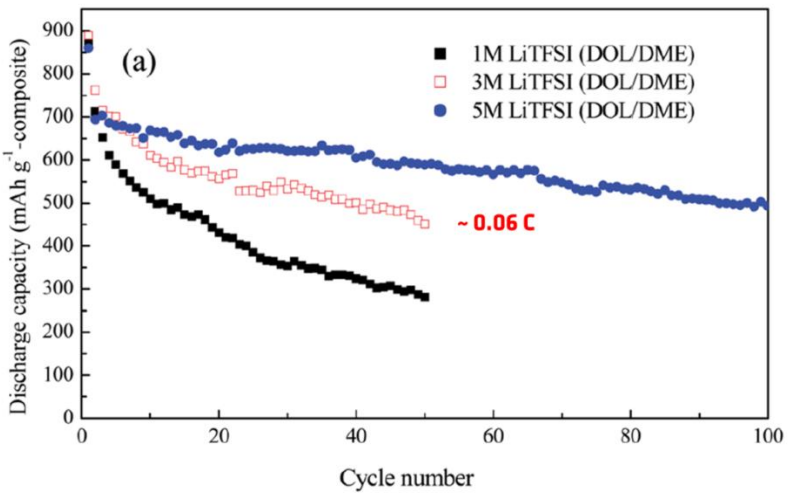

Figure 6 The effect of electrolyte concentration on the cycle stability[20]

It can be a good approach at low C rate by inhibiting the shuttle phenomenon as shown in Fig. 6.

1.2.5. Limitations and summary

For the purpose of alleviating polysulfide shuttle phenomenon, various porous carbon materials were attempted. It did improve the cycle stability of lithium sulfur batteries only if charge/discharge was conducted at low C rate. The issue of rate capability is also the case for lithium sulfur batteries with functionalized carbon materials, physical barrier insertions or solid electrolytes.

Furthermore, insertion of physical barriers is not favorable in terms of the capacity, so called tap density, if the all components are considered. If the weights of additional barriers are considered, the reported capacities are unable to avoid the downward revision. In this reason, additional additives are not favorable.

For the commercialization of lithium sulfur batteries, the capacity should not be drastically faded at moderate charge/discharge rate, for example 1C. Even at high C rate such as 5C, lithium sulfur-batteries should be at least equivalent to the currently used lithium ion batteries.

1.3. State of the art on high rate performance.

Before discussing requirements for lithium sulfur batteries with high rate capability, it is useful to examine “lithium sulfur batteries with high rate capability” as summarized in table 1.

mAh/g	Cycle	C rate	Matrix	S loading method	ref
400	160	6	GO	155C 12h	[22]
600	300	1	GNS	S slurry casting	[19]
700	50	3	MPC + CNT	S in CS2	[23]
600	200	1	rGO + TS	155C 10h + 25Ch 2h	[24]
600	100	3	CNT	Na2S2O3 + HCl	[25]
580	50	2	Carbon Black	Na2S2O3 + HCl	[26]
500	100	1	CNT	Carbothermal reduction of Sulphate	[27]
500	50	3.2	Microporous Carbon Aerogel	149C 6h + 300C 2h	[28]
800	10	5	MPC + CNT	115C 20h 0.5 C/min	[29]
345	100	1	Meso+microporous Carbon	155C 12h	[30]
350	10	5	N doped MPC	$H_2S + 1/2O_2$ -> S + H_2O	[31]
500	10	2	CNT	155C 18h	[32]
450	50	0.5	PAN + CNT	300C 4h	[33]
400	5	3	Graphitic layered hollow carbon	155C 12h	[34]
700	5	1.2	MPC + CNT	200C 5h	[35]

Table 1 State of the art on the LSBs with high rate capability

Various materials especially with high electrical conductivity are utilized. Among them, composites between porous materials and highly conductive material such as CNT showed superior rate capability compared to only synthetic carbon used LSBs such as mesoporous carbon and aerogel. In these composites, CNT seems to play a secondary role of providing electron pathway for active materials while porous materials act as trapper for polysulfides.

In addition, it is noticeable that different kinds of sulfur loading methods for preparing carbon/sulfur composites are utilized. The uniformity of sulfur on carbon matrix might be dependent on the utilized methods.

1.4. Requirements for the high rate capability

In order to achieve high rate capability, mass transfer and charge transfer are needed to be favorable even at fast charge/discharge rate.
For the aspect of mass transfer, it should be favorable for lithium ion with effectively immobilizing polysulfides. Thus, pore size of porous carbon materials are required to be carefully controlled. Electrolyte is also needed to be optimized for the mobility of solvated lithium ions,

but not for polysulfides.

For the aspect of charge transfer, electron is not to be interrupted in its way to the charge transfer sites. Thus, minimum level of electrical conductivity is needed to be satisfied. Sulfur and lithium sulfides are also intimately anchored to carbon matrix during cycling so that there is little barrier for the charge transfer.

Discussed several important points for high rate capability LSBs are summarized in Fig. 7.

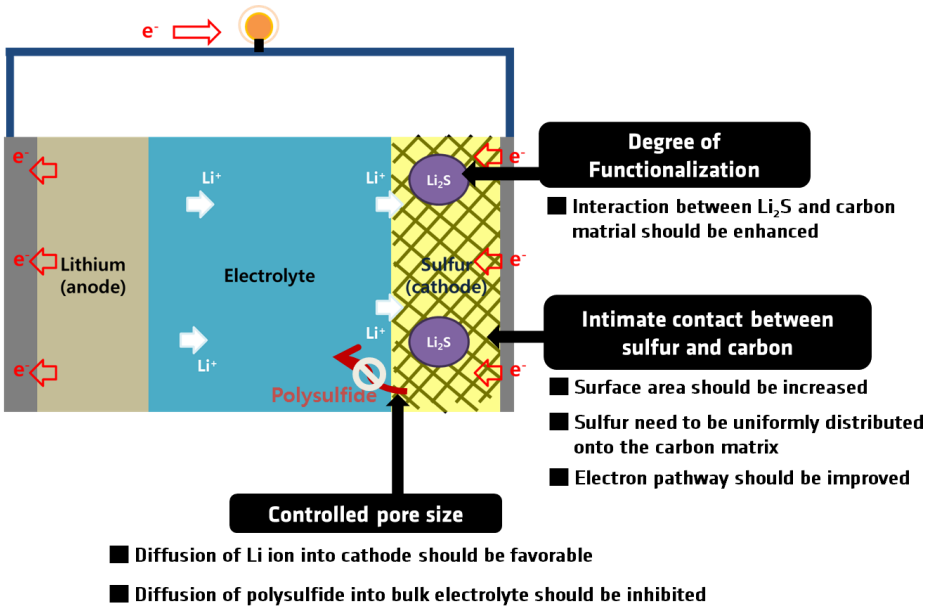

Figure 7 Requirements for high rate capability

There are numerous possible candidate materials for LSBs. Selected candidates which reflect state of the art on LSBs with high rate capability for the carbon matrix are summarized in table 2.

Materials	**BET Surface Area (m^2/g)**	**Pore Volume (cm^3/g)**	**Electrical Conductivity (S/cm)**	**Ref.**
Carbon Blacks	99 ~ 1635	0.01-0.59	$2.0 \sim 10^1$	[36]
rGOs	82 ~ 487	2.61	$4.5 \sim 10^1$	[24, 37, 38]
CNTs	50 ~ 100	0.20	$10^4 – 10^7$	[39]
Templated Carbons	700	0.86	4.6×10^{-8}	[40]
MOFs	1141 ~ 3040	0.84~2.79	5.0×10^{-4}	[41]

Table 2 Candidates for the carbon material

CNTs emphatically show the exceptional electrical conductivity. Due to the limited specific surface area and pore volume, however, it seems not so attractive in LSBs compared to the other options. These demerits might be reasons why CNTs are only likely to play a secondary role as a conductive additive in the composites for high rate capability LSBs.

1.5 Scope and aim of this study

In this study, it has proven that CNT can be modified to an ideal carbon matrix for high rate capability LSBs with sidewall-opened porous CNT/sulfur composite as illustrated in Fig. 8.

By differentiating KOH activation time, the porosity, specific surface area and degree of functionalization were carefully controlled. Analysis on these partially unzipped CNTs was carried out.

Second, the effect of sulfur's uniformity on carbon materials was studied by comparing three different sulfur loading methods.

Finally, the effect of the morphological and chemical changes of CNTs was studied in the aspect of electrochemical performance.

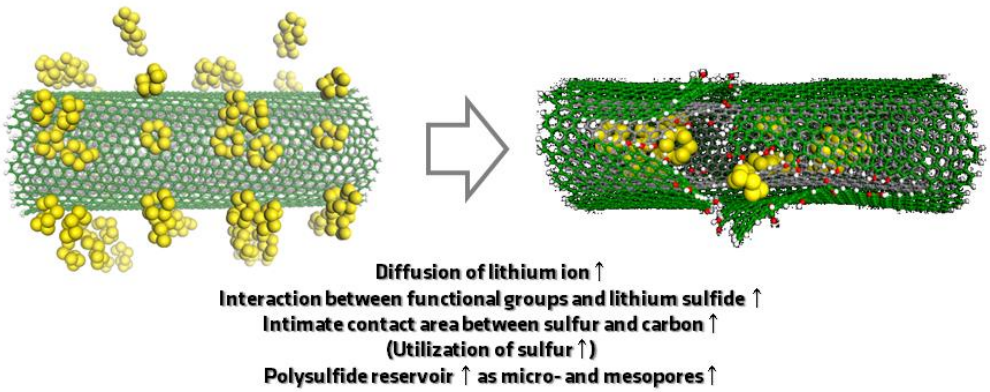

Figure 8 Schematic of the porous CNT and the benefits

2. Experimental

2.1 Reagents and chemicals

As-produced multi-walled carbon nanotubes (CNTs) were purchased from Hanhwa Chemical (Korea). CNTs were synthesized using catalytic chemical vapor deposition process. CNTs were used with purification process. The purification was carried out for 3 hours with mixture of nitric acid and sulfuric acid. Sulfuric acid (concentrated, 95%), nitric acid (14.2 M), hydrogen chloride and potassium hydroxide (pallet, 97% purity) were purchased from Daejung (Korea). Sulfur (reagent grade, powder purified by sublimation) and sodium thiosulfate(reagent grade, 99% purity) was purchased from Aldrich. All materials except CNTs were used without further purification.

2.2 Preparation of porous CNTs (PCNTs)

4 g of potassium hydroxide was dissolved into 50 mL deionized water. Then, 1 g of purified CNT was dispersed into the solution. Before the KOH activation, the solution was stirred for 20 hours on the hotplate of 100 ℃. In order to control the morphological and chemical

characteristics of PCNTs, the KOH activation reaction was carried out for 1h, 2h, 3h and 6h in nitrogen filled tube furnace and then naturally cooled to room temperature (denoted PCNT(1h), PCNT(2h), PCNT(3h), PCNT(6h) respectively). The PCNTs were thoroughly rinsed with deionized water and ethanol with filtering, then dried at 60 ℃ vacuum oven.

2.3 Preparation of PCNT/sulfur composites

To study the effect of sulfur's uniformity, CNT/sulfur composites were prepared by three different methods. The commonly used 'melt diffusion' method was used in the argon filled autoclave at 155 ℃ for 12 hours (denoted as CNT-S_heat). Solution based precipitation reaction between sodium thiosulfate and hydrogen chloride was also utilized (denoted as CNT-S_sol). Finally, combined method of the two was also tried out (denoted as CNT-S_sol + heat).

PCNT/sulfur composites were prepared by the combined method. First, sodium thiosulfate was dissolved into deionized water. Then, PCNT powder was dispersed in the solution. 1 M of hydrogen chloride was slowly added to the solution drop by drop. After overnight stirring,

the solution is washed up with deionized water and ethanol several times. Prepared PCNT/sulfur composites were dried at 60 ℃ vacuum oven overnight, followed by heat treatment in the argon filled autoclave at 155 ℃ for 12 hours. The sulfur cathodes were all prepared by doctor blade coating method with polyvinylidene (10 wt%), carbon black(10 wt%) and active material(80 wt%). The electrolyte was 1 M of LiTFSI in DME/DOL (1:1 of volume ratio) solution added with 0.25 M of $LiNO_3$

2.4 Characterization

The morphologies of the prepared samples were examined with a field-emission scanning electron microscope (FE-SEM; JSM-6700F, JEOL) and a transmission electron microscope (TEM; JEM-2100F and JEM-3000F, JEOL). The microstructures of the samples were also investigated with powder X-ray diffraction (XRD; D8 Advance diffractometer, Bruker) in the reflection mode of Ni-filtered CuKα radiation (λ=0.154184 nm). X-ray photoelectron spectroscopy (XPS, AXIS-His, Kratos) and Raman spectroscopy (Ramanplus, Nanophoton) with laser wavelengths between 532 and 785 nm were utilized in

analysis of surface characteristics of the samples. The Specific surface area and pore distribution of the samples were calculated based on the BET equation, and the nitrogen adsorption data was measured by Micromeritics ASAP 2020. Thermogravimetric analysis(TGA; SDT Q600, TA) was carried out.

2.5 Electrochemical experiment

The electrochemical test was conducted using a battery cycler (WBCS3000, WonATech). The prepared samples were fabricated into the 2032 coin-type half-cell in the Ar-filled glove box (Korea Kiyon). The electrochemical performances of samples were based on the mass of sulfur and measured in the potential range of 1.5-2.8 V vs Li/Li^{+}. In addition, the contents of sulfur in prepared PCNT/sulfur and CNT/sulfur composites were calculated based on the thermogravimetric analysis (TGA).

3. Results and Discussion

3.1 Analysis on PCNTs

3.1.1 Morphological characteristics

As KOH activation time increased, the walls of purified CNT were damaged and partially ripped. The morphological structure changes were observed by transmission electron microscopy (TEM) as shown in Fig. 9. The walls of purified CNT were smooth and the tubular structures are well preserved. The diameters of purified CNT were around 20-30 nm as shown in Fig. 9 (a).

The TEM images of PCNTs in Fig. 9 (b), (c), (d) and (e) showed that partially ripped part of the CNT walls was successfully confirmed. The ripped part of PCNTs looked like nano ribbon (NR) as marked as red arrows in Fig 9, while other parts of PCNTs preserved the nano-tubular morphologies even after the severe condition of KOH activation.

However, PCNT(3h) and PCNT(6h) were differentiated from PCNT (1h) and PCNT (2h) in that the NR-like ripped parts were twisted and less clear in PCNT (3h) and PCNT (6h). This might be originated from the prolonged severe condition of KOH activation.

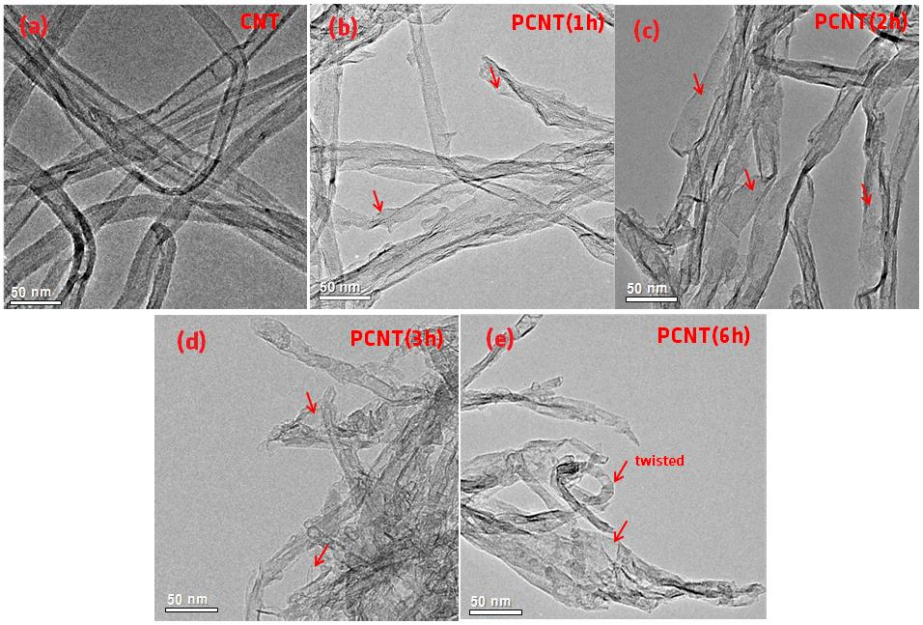

Figure 9 TEM images of CNT and PCNTs based on KOH activation time for (a) CNT, (b) 1 hour activation, (c) 2 hour activation, (d) 3 hour activation, and (e) 6 hour activation

Physical natures of the samples such as specific surface area and pore volume were also examined by the nitrogen adsorption and desorption isotherm. As illustrated in Fig. 11, Brunauer-Emmett-Teller (BET) specific surface area of purified CNT (50.98 m^2/g) is highly increased via KOH activation up to 504.48 m^2/g of PCNT(3h). The specific surface area tends to increase as treatment time goes except PCNT (6h). This increase of specific surface area might be originated from the opening the closed structure of CNT which made inner side of CNT available.

However, decrease in PCNT (6h) compared to other PCNTs might be explained by the loss of damaged carbon fragments in the process of rinsing and filtering after activation treatment. It can be inferred from the TEM image of residual after filtering the PCNT samples. As observed the lattice of carbon nanotube in Fig. 10, small fragments produced during KOH activation were rinsed out from the PCNTs which dispersed in de-ionized water and ethanol. This CNT fragments dispersed solution was highly produced especially after 6 hour treatment.

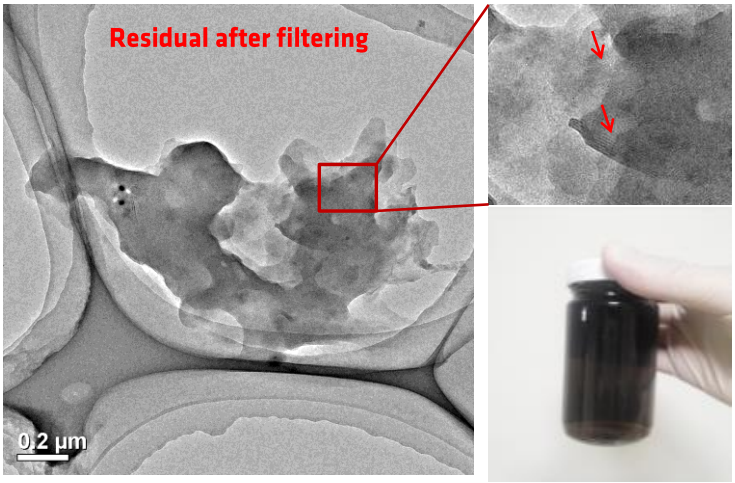

Figure 10 TEM images of residual after filtering PCNT (6h) and picture of overlapped CNT fragments in the dispersed solution

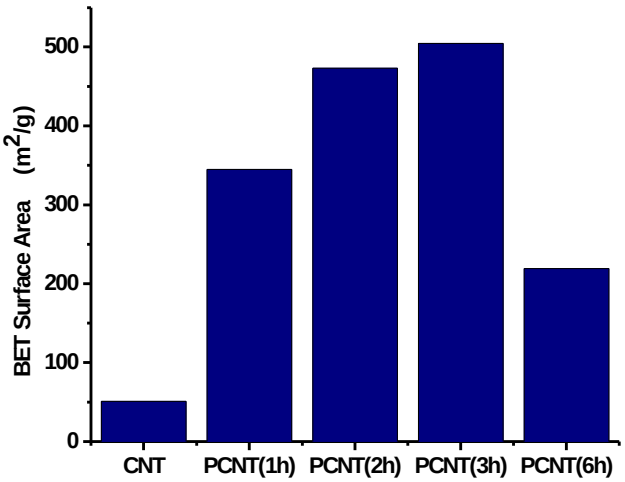

Figure 11 Brunauer-Emmett-Teller (BET) specific surface areas

Based on the BET specific surface area, the thickness of sulfur loaded on CNT and PCNTs can be calculated. The uniform coating of sulfur 1 g on 1 g of the carbons is assumed. The calculation was based on the followed equation.

$$Thickness\ of\ sulfur = \frac{Volume\ of\ 1\ g\ sulfur}{Specific\ surface\ area\ of\ 1\ g\ carbons}$$

Sample	Thickness of 1g S on 1g of PCNT
CNT	9.5 nm
PCNT (1h)	1.4 nm
PCNT (2h)	1.0 nm
PCNT (3h)	1.0 nm
PCNT (6h)	2.2 nm

Table 3 Calculated the thickness of sulfur on the carbons on the assumption of uniform coating

The thickness of sulfur on the carbon matrix reflects the electron penetration depth for the redox reaction. As summarized in Table 3, the thicknesses of PCNT (2h) and PCNT (3h) samples were the lowest value of 1.0 nm due to the high specific surface areas.

Pore volumes of the samples were measured from 1.7 nm to 300 nm diameters of pores. The values are summarized in Fig. 12. It is worth to note that PCNT (3h) which showed the highest value of specific surface area had relatively lower value of pore volume, 0.50 cm^3/g. However, PCNT (2h) sample with almost same value of specific surface area with PCNT (3h) had the largest value of pore volume. This might be interpreted the increase of micropores below 1.7 nm which cannot be detected from the N_2 adsorption and desorption isotherm. This means that volume of micropores in PCNT (3h) is larger than that in PCNT (2h).

The amount of sulfur or lithium sulfide in order to fill up the measured pores of PCNT samples was calculated on the basis of followed equation. The uniform and homogenous loading of sulfur and lithium sulfide on pores of 1g of PCNTs was assumed.

$$\textit{The amount of Sulfur} = \textit{Pore volume of PCNT} \times \textit{Density of Sulfur}$$

$$\textit{The amount of } Li_2S = \textit{Pore volume of PCNT} \times \textit{Density of } Li_2S$$

The calculated amounts of lithium sulfide or sulfur to fill up the pores of 1 g PCNTs are important in that excessive sulfur loading over

the available pore volume of PCNT can increase the chance of blocking the pathway into the pore with discharged product, lithium sulfide.

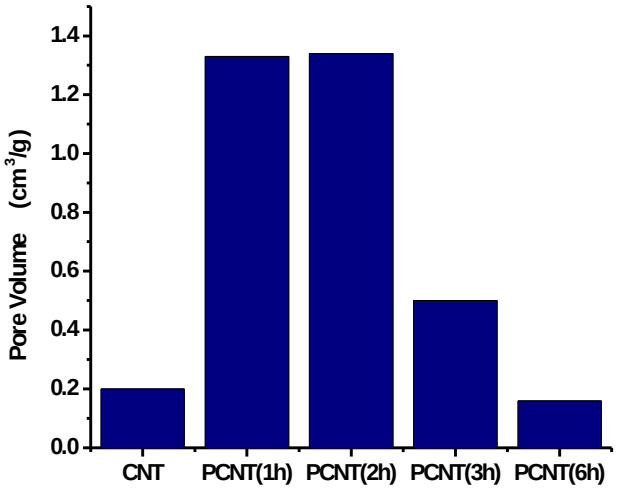

Figure 12 Pore volumes of CNT and PCNTs

Sample	Li_2S per 1g of PCNT	S per 1g of PCNT
PCNT (1h)	2.21 g	1.54 g
PCNT (2h)	2.22 g	1.55 g
PCNT (3h)	0.83 g	0.58 g
PCNT (6h)	0.27 g	0.19 g

Table 4 Calculated amounts of lithium sulfide or sulfur in order to fill up the pores of 1 g PCNT

3.1.2 Chemical surface characteristics

The surface characteristics of the PCNTs were analyzed with XPS and Raman spectroscopy. By using Raman spectroscopy, I_D/I_G ratios were calculated from the peak intensities of the D-band at about 1330 cm^{-1} and G-band at about 1588 cm^{-1}. Defects and disorder in the carbons are related to the D-band, and their concentrations affect the intensity of D-band.[42]

In Fig. 13, I_D/I_G ratios were calculated from Raman spectrums of purified CNT and PCNTs. The degree of disorder on the carbon backbone was increased as the activation time increased, however it was saturated around 3 hour treatment. This indicates that defects were continuously generated, however after 3 hour activatioin the highly damaged graphitic structures of CNT broke into small CNT fragments which were filtered out from the sample during the rinsing process as mentioned above with Fig. 10. The saturation of defects, the degree of disorder, at the surface of PCNTs originated from the rinsing process.

The chemical surface nature of PCNTs was understood using XPS. As illustrated Fig. 14 and 15, the degree of functionalization was increased with the KOH activation time before 3 hour. In PCNT(6h),

the degree of functionalization was decreased about 1.7 % compared to the PCNT(3h).

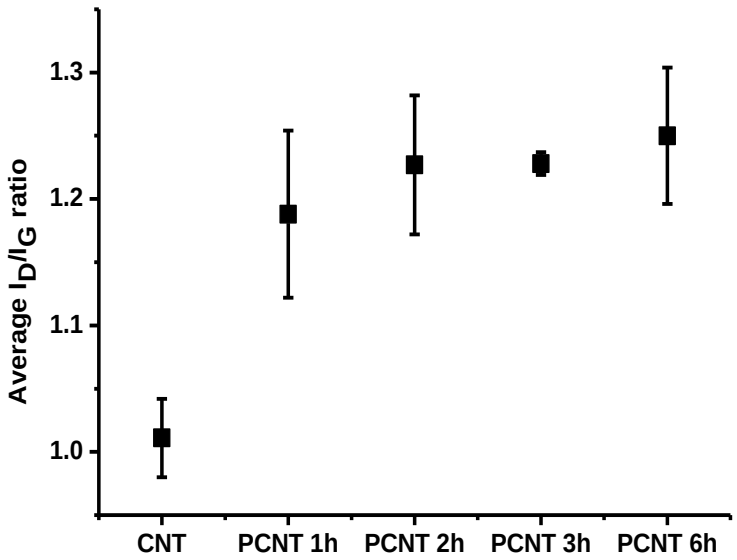

Figure 13 I_D/I_G ratios of purified CNT and PCNTs

By deconvoluting C1S peaks of PCNTs, I was able to investigate the chemical states of PCNTs. C=C (284.4 eV), C-C (285.1 eV), C-O (286.2 eV), C=O (287.4 eV) and O-C=O (289.1 eV) were analyzed. After deconvolutin C1S peaks, the data was converted into a fraction of each functional group and illustrated as bar graph in Fig. 15. As you can see the fraction of each functional group also increased with the

activation time and saturated at 3 hours. This trend is consistent with that of O/C ratio. C-O fraction is higher than others. As hydroxyl groups are known as an effective functional group which interacts with polysulfide, highly functionalized PCNTs were expected to show good electrochemical performance by trapping polysulfide.[17]

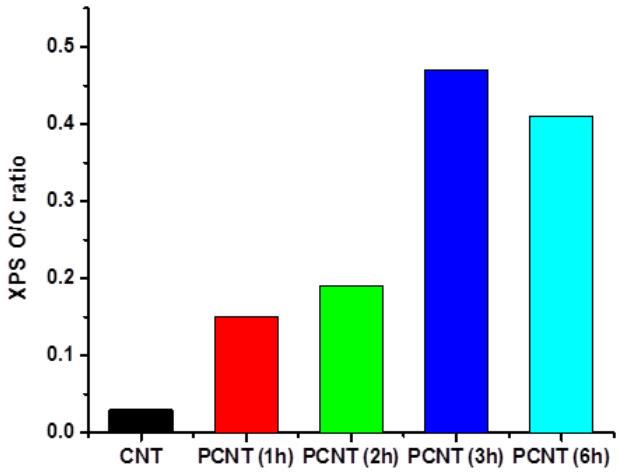

Figure 14 O/C ratios of purifed CNT and PCNTs

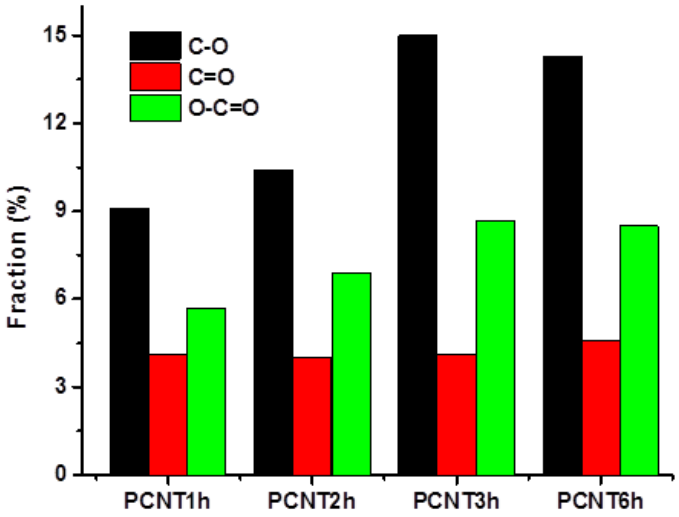

Figure 15 Fraction ratios from deconvoluted XPS peaks

3.2 Study on the effect of uniform sulfur distribution for the preparation of PCNT/sulfur composites

3.2.1 Morphological, microstructural and thermal characteristics

Before preparing PCNT/sulfur composites, it is required to find out what is the best adequate method for uniform distribution of sulfur on carbon matrix, because the uniformity of sulfur on carbon matrix is depending on how carbon/sulfur composite prepares. CNT/sulfur composites were studies for the purpose, instead of PCNT/sulfur composites. CNT/sulfur composites were prepared by three different methods: solution based precipitation method, commonly used melt diffusion method, and combined method of the two.

TEM images of prepared three different CNT/sulfur samples are shown in Fig. 16. In the TEM images of CNT-S_Heat and CNT-S_Sol samples, the big chunk of sulfur particles were observed. The size of sulfur particles were around 100 nm width in CNT-S_Sol sample. In the CNT-S_Sol+Heat sample prepared by the combined methods, however, huge aggregations of sulfur particles were not observed. As shown in Fig 16, sulfur was uniformly distributed in CNT-S_Sol+Heat sample.

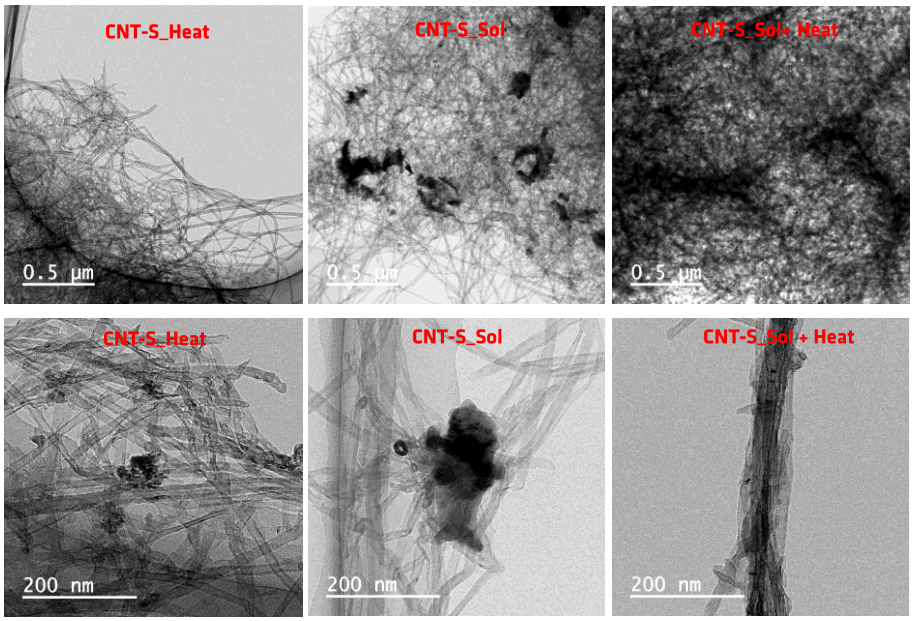

Figure 16 TEM images of prepared CNT/sulfur composites

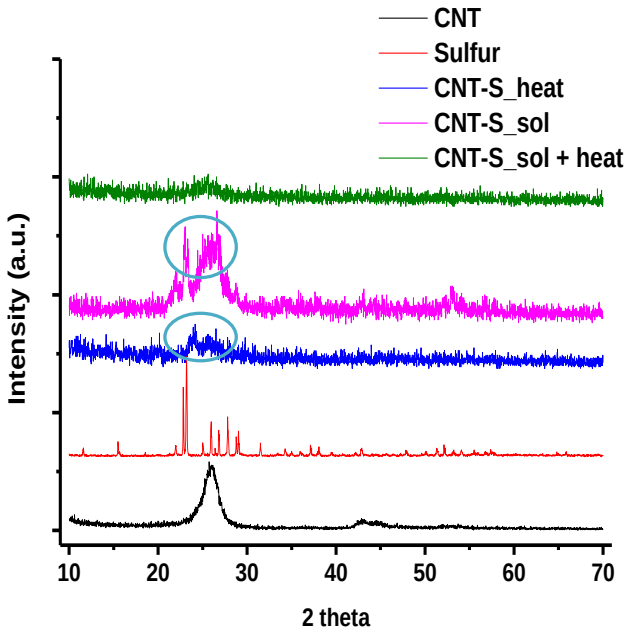

Figure 17 XRD patterns of CNT/sulfur composites, CNT and sulfur

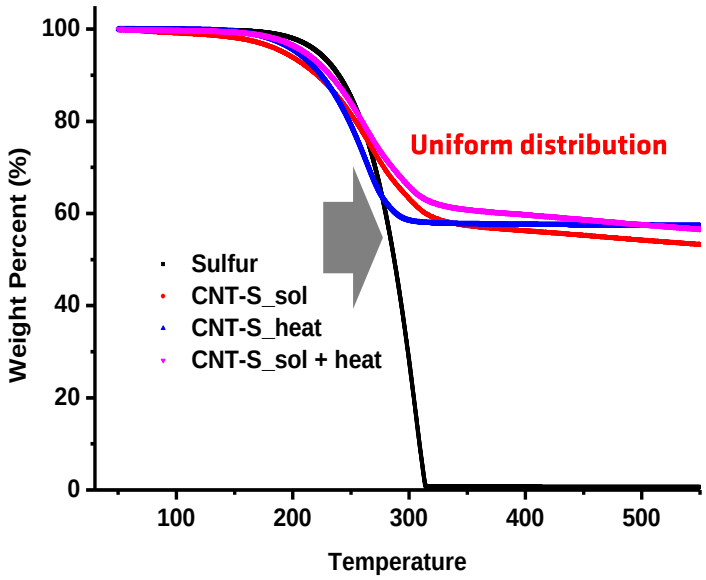

Figure 18 Thermogravimetric analysis (TGA) of prepared samples and as-purchased sulfur powder

XRD patterns of prepared CNT/sulfur composites, CNT and as-purchased sulfur powder were illustrated in Fig. 17. The sharp characteristic peaks of α-sulfur which is stable phase at room temperature are appeared between 20° and 30°. In CNT-S_sol and CNT-S heat samples, the characteristic peaks of α-sulfur were observed. This demonstrated the presence of large crystal of sulfur in the CNT-S composites.

On the other hand, obvious characteristic peaks of sulfur were not detected in the CNT-_sol + heat sample. This can be interpreted as complete infiltration into pores without bulk crystalline sulfur. The sulfur content can be determined by thermogravimetric analysis (TGA).[10] Because the boiling temperature of sulfur is 444.6 ℃, the sulfur in the carbon matrix is completely vaporized at 500 ℃. Assuming that the mass of carbon matrix does not diminish, sulfur content is easily calculated from Fig. 18. Sulfur contents in CNT-S_Sol, CNT_Heat, and CNT-S_Sol+Heat are 46 wt.%, 43 wt.% and 43 wt.% respectively. It is also worth to note that the weight of CNT_Sol+Heat was slowly diminished compared to others. This also supports the uniform sulfur loading in the matrix of CNT, because uniform distribution of sulfur on carbon matrix enhances the interaction between sulfur and carbon. As discussed above, it is able to evaluate sulfur infiltration methods using TGA.[43]

From the visual investigation and thermal stability analysis on CNT/sulfur composites, it is able to conclude that the combined method is effective in uniform distribution of sulfur on the carbon matrix, especially CNT.

3.2.2 Electrochemical performance of CNT/sulfur composites depending on the uniformity of sulfur

The electrochemical performances of CNT/sulfur composites prepared by three different methods were investigated at low charge/discharge rate, 0.2 C. As shown in Fig. 19 and Fig. 20, CNT-S_Sol+Heat sample gave the superior specific discharge capacity compared to the other samples. The 1st specific discharge capacities of CNT-S_Sol+Heat, CNT-S_Sol and CNT-S_Heat were measured as 592, 253 and 172 mAh/g at 0.2 C, respectively. After 50 cycles, the specific discharge capacities of CNT-S_Sol+Heat, CNT-S_Sol and CNT-S_Heat were decreased to 311, 97 and 136 mAh/g, respectively. In addition, Coulombic efficiency of CNT-S_Sol+Heat indicated nearly 100 % with great stability compared to others as shown in Fig. 20.

These results support that uniformly sulfur distributed CNT matrix leads to a relatively good performance compared to CNT matrix with bulk sulfur crystalline aggregations. PCNT/sulfur composites were prepared by the combined method, heat treatment at 155 ℃ for further uniform distribution of sulfur after precipitation of small sulfur particles on carbon matrix.

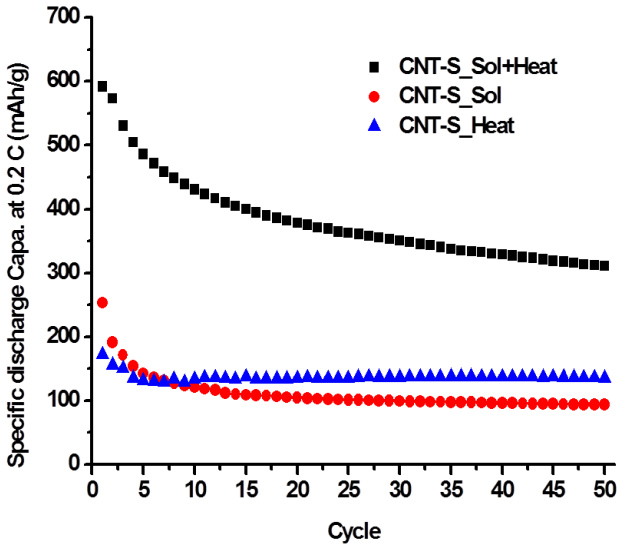

Figure 19 Cycle performances of CNT/sulfur composites at 0.2 C

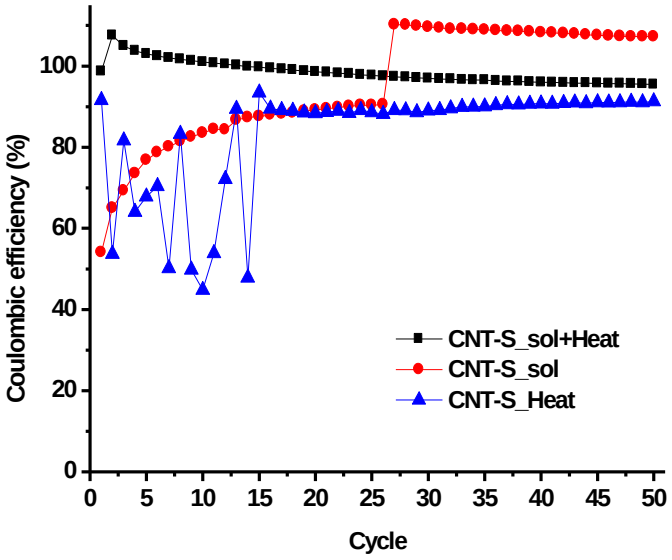

Figure 20 Coulombic efficiencies of CNT/sulfur composites at 0.2 C

3.3 Analysis on PCNT/sulfur composites

3.3.1. Visual investigation on PCNT/sulfur composites

Fig. 21 shows the morphologies of PCNT/sulfur composites were prepared by the combined method. Tubular structure of CNT was preserved in the FE-SEM images of PCNT/sulfur samples. In addition, the bulk sulfur crystalline aggregations were not observed in the PCNT/sulfur composites as you can notice in Fig. 21. In all the PCNT/sulfur samples, it seemed that sulfur was uniformly distributed on the carbon matrix.

According to Fig. 22, TEM image of the PCNT (2h)/sulfur composite provides the evidence that sulfur was partially filled in the inner pores and the opened sidewalls of CNT. By giving lithium ion room to diffuse in and out, sulfur in the inner pore of PCNT is able to be participated in the redox reaction. Compared to sulfur in CNT samples as shown in Fig. 16, uniformity of sulfur was well realized in PCNT/sulfur with partially filled inner pore of PCNT.

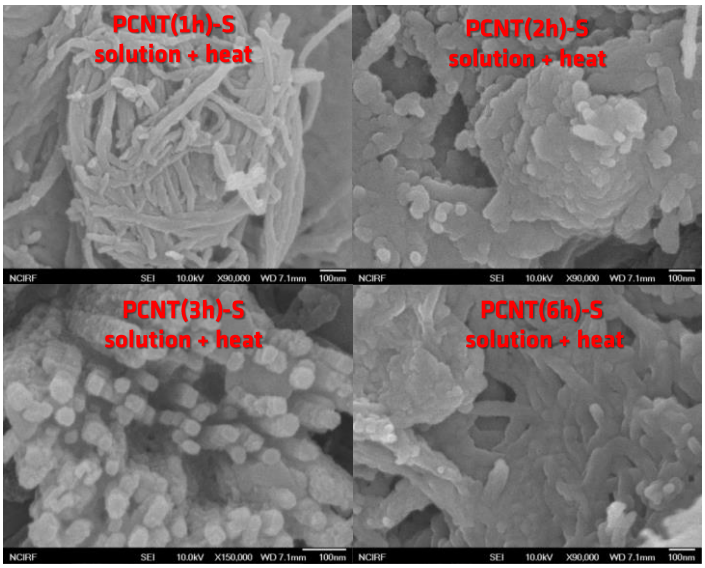

Figure 21 FE-SEM images of the PCNT/sulfur composites

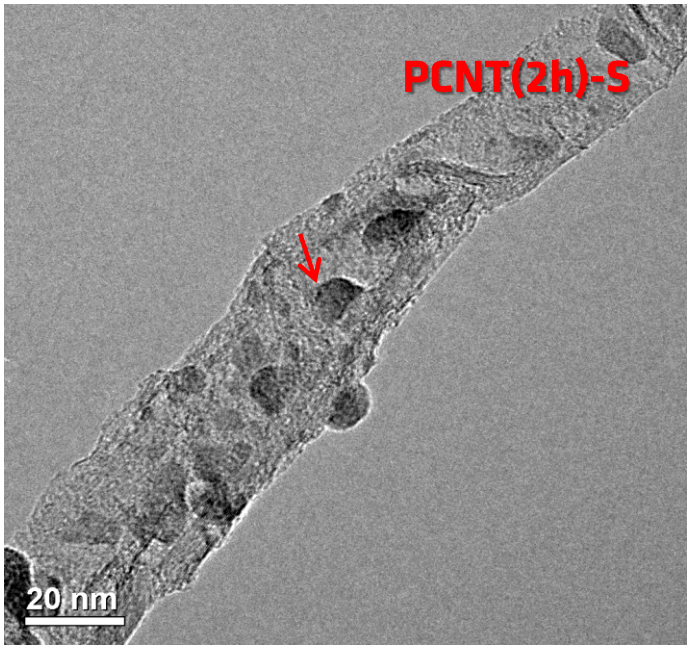

Figure 22 TEM images of the PCNT(2h)/sulfur composite

3.3.2 Microstructural analysis and thermal stability of PCNT/ sulfur composites

The XRD patterns of PCNT/sulfur composites offer the information about the uniform distribution of sulfur on PCNT as presented in Fig. 23. There was no clear evidence of sharp characteristic peaks of crystalline sulfur between 20° and 30° which are clearly detectable in the as-purchase sulfur as you can find in Fig. 17. It can be concluded that sulfur had been well infiltrated into the inner pore and uniformly distributed onto the carbon matrix of PCNTs.

It is also worth to note that (002) peak of CNT at 26.6° was remained in all the PCNT/sulfur composites even though harsh KOH activation was conducted. The existence of (002) peak reflects the graphitic nature of MWCNT.[44] On the other hand, (101), (004), and (110) peaks of CNT were weak and hard to be recognized from the noise signal.

The measured XRD patterns of PCNT/sulfur composites indicating clear observation of (002) peak are consistent with the FE-SEM and TEM images of PCNTs and PCNT/sulfur composites that showed preserved tubular structure.

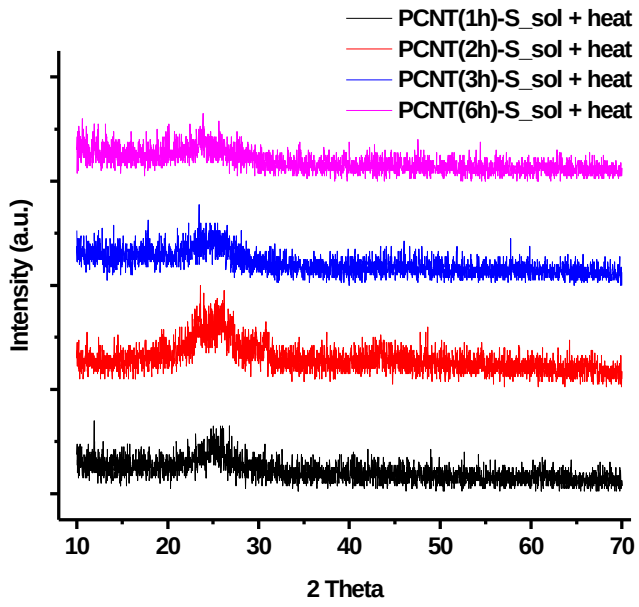

Figure 23 XRD patterns of PCNT/sulfur composites

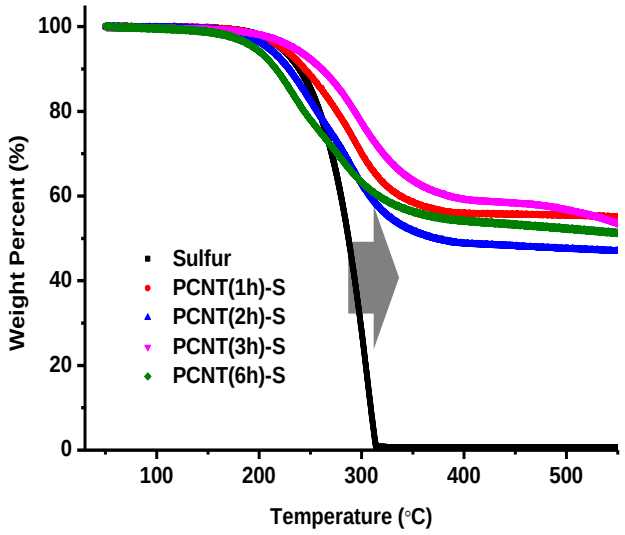

Figure 24 TGA of PCNT/sulfur composites and as-purchased sulfur

The sulfur contents and the thermal stability of sulfur in PCNT/sulfur composites were investigated with TGA, as shown in Fig. 24. The TGA data of PCNT (1h)-S, PCNT (2h)-S, PCNT (3h)-S and PCNT (6h)-S samples gave sulfur contents of 46, 51, 42, and 47 wt.%, respectively.

The thermal stability of sulfur in PCNTs was enhanced compared to the thermal stability of sulfur. Pure sulfur in the absence of the interaction with carbon matrix relatively vaporized at rapid speed and completely disappeared at early temperature than the sulfur in PCNT composites. The analysis with TGA was already conducted in other previous report for the indicator of whether the location of sulfur was in the pore of porous materials or not.[45]

3.4 Electrochemical performance of PCNT/sulfur composites

3.4.1. Cycle performances of PCNT/sulfur composites

The electrochemical performance of PCNT/sulfur composites and the reference, CNT/sulfur composite prepared by the combined method were examined at different two charge/discharge rates, 0.2 C and 5 C. (1 C = 1675 mA/g) The summarized results of the different C rate tests are tabulated in Table 5 and 6, respectively.

0.2 C	PCNT(1h)-S	PCNT(2h)-S	PCNT(3h)-S	PCNT(6h)-S
1st	1265.9	1301.8	1240.6	1138.0
50th	681.0	718.7	594.5	595.7
Retention	53.8	55.2	47.9	52.3

Table 5 Summarized specific discharge capacity of PCNT/sulfur composites at low C rate, 0.2 C

5 C	PCNT(1h)-S	PCNT(2h)-S	PCNT(3h)-S	PCNT(6h)-S
1st	612.3	688.5	640.4	289.2
50th	486.2	671.8	531.6	228.1
Retention	79.4	97.6	83.0	78.9

Table 6 Summarized specific discharge capacity of PCNT/sulfur composites at high C rate, 5 C

The cycle performances of PCNT/sulfur composites and the reference at low C rate, 0.2 C and high C rate, 5C were shown in Fig. 25 and Fig. 26, respectively. The PCNT (2h)-S performed the best result at low C rate test. The initial discharge capacity of PCNT (2h)-S was 1265.9 mAh/g and delivered 718.7 mAh/g after 50 cycles. On the other hand, the CNT/sulfur composite only delivered 591.9 mAh/g at the first discharge and diminished into 310.6 mAh/g. PCNT (2h)-S increased the initial specific discharge capacity at low C rate. Of course, the other PCNT/sulfur composites enhanced the electrochemical performances compared to the reference.

At high C rate of 5 C, the reference CNT/sulfur composite cell was inactivated due to the overwhelmingly rapid charge/discharge rate. The specific capacity of the reference cell was given in zero. On the other

hand, the PCNT/sulfur composites provided superior electrochemical performances. The PCNT (2h)-S also performed the best at even high C rate. The first specific discharge capacity of PCNT (2h)-S was measured as 688.5 mAh/g and delivered 671.8 mAh/g after 50 cycles. The specific discharge capacity of PCNT (2h)-S at high C rate was just 46.9 mAh/g lower than the result at low C rate, even though the C rate was 25 times speeded up. This remarkable improvement was not the case in the reference cell. Unable to withstand the rapid speed, it just inactivated.

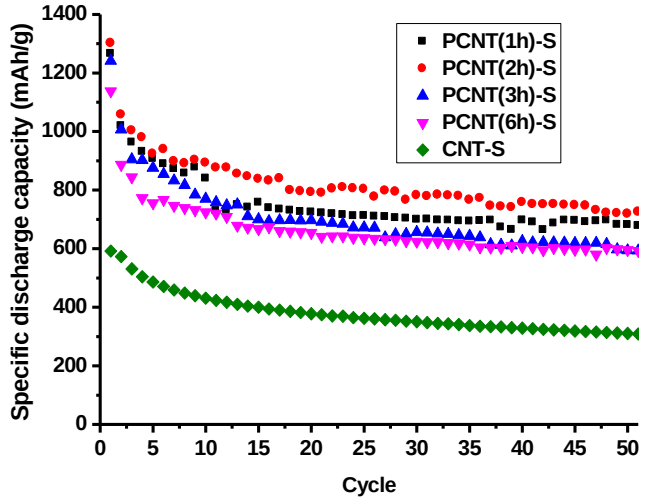

Figure 25 Specific discharge capacity of PCNT/sulfur composites and the reference at 0.2 C

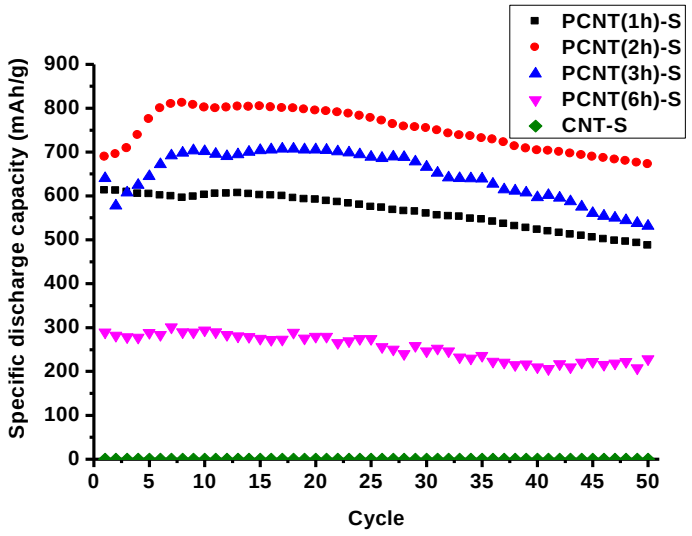

Figure 26 Specific discharge capacity of PCNT/sulfur composites and the reference at 5 C

3.4.2 The effects of material properties on the electrochemical performances

The remarkable improvements of electrochemical performances even at very rapid 5 C might be originated high specific surface area, large pore volume with functional groups of PCNT/sulfur composites. It should be required for further optimizations and improvements in electrochemical performances to discuss the effects of individual factors: specific surface area, pore volume and degree of functionalization.

The specific surface area affects the electron penetration depth from the carbon matrix to sulfur at discharge state, as illustrated in Fig. 27.

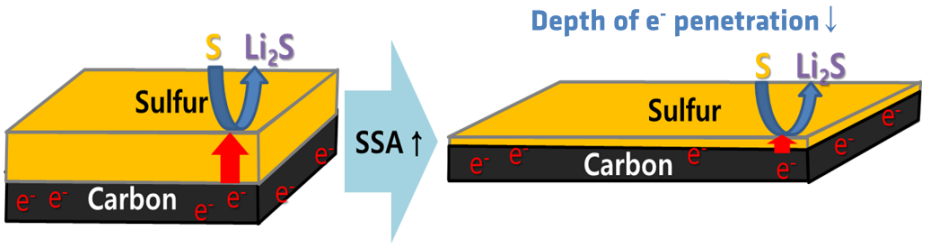

Figure 27 The effect of specific surface area of carbon matrix

If the specific surface area is enlarged, then the electron penetration depth is shortened. This leads to the reduced cell resistance and enhanced kinetics of the redox reaction of sulfur. As shown in Fig. 28, the correlation between the specific capacity and the specific surface area was demonstrated except a little deviation at PCNT (3h) sample. This deviation can be explained by considering the lithium ion diffusion pathway. As summarized in Table 3, the calculated electron penetration depth is the shortest in PCNT (2h) and PCNT (3h) due to the high specific surface area.

The lithium ion diffusion pathway, however, is guaranteed in PCNT (1h) and PCNT (2h) instead of PCNT (3h) due to the size of pore volume, as you can see in Table 4. Considering the electron penetration depth and room for lithium ion diffusion pathway, the superior electrochemical performance of PCNT (2h)/sulfur sample is justifiable.

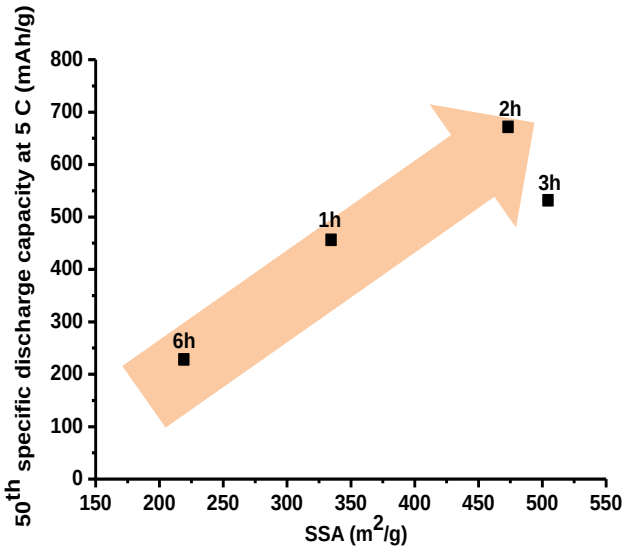

Figure 28 The correlation between the 50th specific capacity and the specific surface area

The good retention of PCNT/sulfur composites are also explained by the effect of porous carbon in trapping polysulfide as illustrated in Fig. 29.

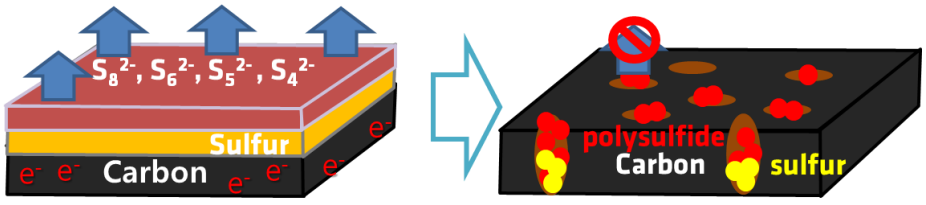

Figure 29 The effect of porous carbon in trapping polysulfide

Providing room for lithium ion diffusion pathway is related to the pore volume of carbon matrix and the amount of infiltrated sulfur. As illustrated in Fig. 30, lithium sulfide is likely to block the pores during the discharge if the pore volume is fully loaded with sulfur.

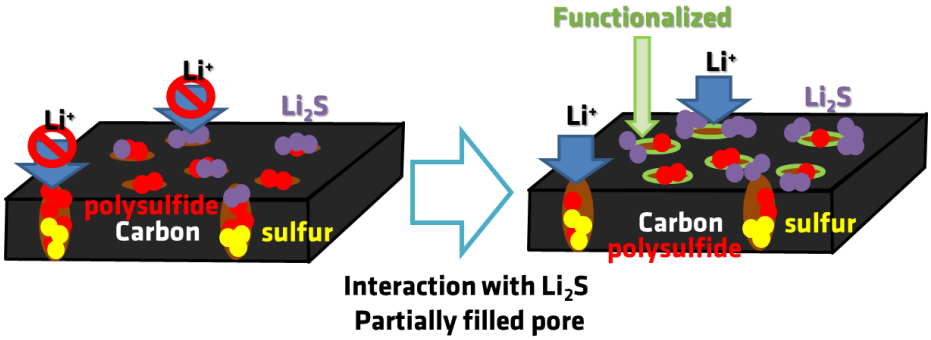

Figure 30 The effect of partial loading of sulfur with the functional groups on the carbon matrix

For further investigation of the effect of functional groups on PCNT, the PCNT (1h) sample was reduced under the flow of inert nitrogen gas at 500 ℃ for 3 hours. Fig. 31 confirmed that the degree of functionalization was diminished after the reduction on PCNT (1h).

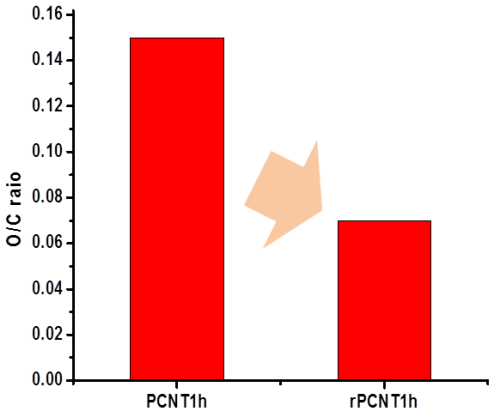

Figure 31 The diminished O/C ratio of PCNT (1h) after the reduction

The electrochemical performances of PCNT (1h)/sulfur and reduced PCNT (1h)/sulfur (R.PCNT (1h)/sulfur) composites were summarized in Fig. 32. At both of the low C rate of 0.2 C and the high C rate of 2 C, R.PCNT (1h)/sulfur composite alleviated the polarization at the first cycle. The reduced polarization improved the Coulombic efficiency of the sample compared to PCNT(1h)/sulfur composites.

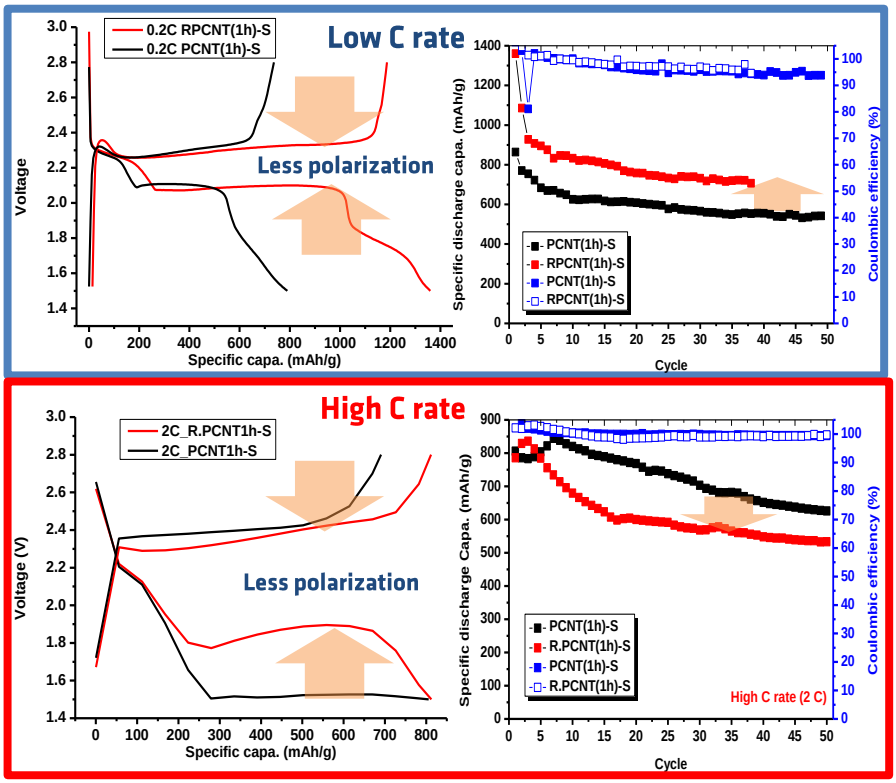

Figure 32 The effect of the functional groups on PCNT(1h)/sulfur composite at low and high C rates

However, the cycle performances of the R.PCNT (1h)/sulfur composite were depending on the C rate. At the low C rate, the reduction improved the specific discharge capacity. It might be originated from the enhanced electrical conductivity of the carbon matrix.

At the high C rate, on the other hand, the specific discharge

capacity was deteriorated compared to PCNT (1h)/sulfur. It demonstrated that the existence of functional groups seemed to be more important in trapping polysulfide and alleviating the aggregation of lithium sulfide rather than the electrical conductivity.

It is also worth to mention that the effect of functionalization is only meaningful under the condition of guaranteed marginal electrical conductivity. Because CNTs had superior electrical conductivity compared to other carbon materials as discussed with Table 2, the effect of functionalization is guaranteed.

Thus, further functionalization of carbon matrixes can be of great help to improve the high rate performance of lithium sulfur batteries in the case of high electrical conductivity carbons such as CNT and graphene.

3.4.3 The electrochemical impedance spectroscopy analysis of PCNT/sulfur composites

The Nyguist impedance spectra of the PCNT/sulfur composites and CNT/sulfur composite are illustrated in Fig. 33. It can be clearly seen that the PCNT/sulfur composites had smaller resistance of the coin cells than the CNT/sulfur composite, even though pristine CNT showed higher electrical conductivity of CNT itself. This is due to the fact that sulfur was well distributed on PCNTs with the shortened electron penetration depth as discussed in 3.1.1.

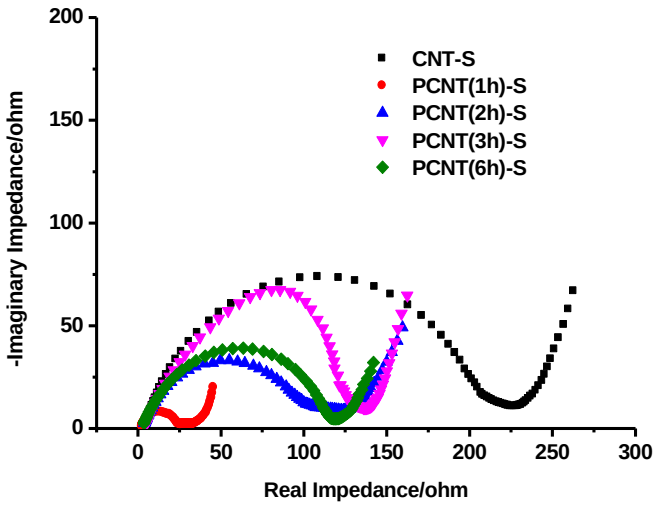

Figure 33 Nyguist impedance spectra of the PCNT/sulfur composites and CNT/sulfur composite

3.5 Further works

In this study, it was demonstrated that the specific surface area, pore volume, and functional groups of PCNTs had great impact on the electrochemical performances of the samples. It is expected that the porous CNTs can be further ripped into nano ribbon (NR) with additional treatments. There might be additional electrochemical performance change by this morphological change from porous CNT to fully ripped CNT, NR.

Furthermore, the chemical surface nature of porous CNT (PCNT) is able to be further controlled in order to improve the electrochemical performances. The effects of diameter and wall numbers of CNT are also able to be examined to further improve the electrochemical performance.

In addition, this study is also applicable to other energy storage systems such as supercapacitors or pseudocapacitors. The effects of material characteristics can be further studied in those fields.

4. Conclusion

In this study, porous CNTs were successfully prepared and proven to have high SSA, large pore volume and functional groups via the facile way, KOH activation. Porous CNT (2h) especially showed the highest performance of 718 mAh/g at 5 C due to shorten electron penetration depth and guaranteed lithium ion diffusion pathway.

It was also demonstrated that large SSA is effective in shorten electron penetration depth and large and pore volume guarantees lithium ion diffusion pathway. It was also found that the effect of functional groups is depending on charge/discharge rate. At high C rate, the effect of functional groups on polysulfide dissolution issue is important due to the fast electron supply from the carbon matrix compared to the situation at low C rate. The electrical conductivity is more important at low C rate. In addition, the effect of uniformity of sulfur on the carbon matrix is also discussed.

By designing and studying the suitable carbon matrix for high rate capability lithium sulfur batteries, I believe, we are stepping forward to the commercialization of lithium sulfur batteries.

5. Reference

1. Yin, Y.-X.; Xin, S.; Guo, Y.-G.; Wan, L.-J. *Angewandte Chemie International Edition* **2013,** 52, (50), 13186-13200.
2. Song, M.-K.; Cairns, E. J.; Zhang, Y. *Nanoscale* **2013,** 5, (6), 2186-2204.
3. D. Herbert, J. U. Electric dry cells and storage batteries. 1962.
4. Manthiram, A.; Fu, Y.; Su, Y.-S. *Accounts of Chemical Research* **2012,** 46, (5), 1125-1134.
5. Mikhaylik, Y. V.; Akridge, J. R. *Journal of The Electrochemical Society* **2004,** 151, (11), A1969-A1976.
6. Barchasz, C.; Molton, F.; Duboc, C.; Leprêtre, J.-C.; Patoux, S.; Alloin, F. *Analytical Chemistry* **2012,** 84, (9), 3973-3980.
7. Yeon, J.-T.; Jang, J.-Y.; Han, J.-G.; Cho, J.; Lee, K. T.; Choi, N.-S. *Journal of The Electrochemical Society* **2012,** 159, (8), A1308-A1314.
8. Walus, S.; Barchasz, C.; Colin, J.-F.; Martin, J.-F.; Elkaim, E.; Lepretre, J.-C.; Alloin, F. *Chemical Communications* **2013,** 49, (72), 7899-7901.
9. Diao, Y.; Xie, K.; Xiong, S.; Hong, X. *Journal of The Electrochemical Society* **2012,** 159, (4), A421-A425.
10. Ji, X.; Lee, K.; Nazar, L. *Nat Mater* **2009,** 8, 500 - 506.
11. Oschatz, M.; Borchardt, L.; Pinkert, K.; Thieme, S.; Lohe, M. R.; Hoffmann, C.; Benusch, M.; Wisser, F. M.; Ziegler, C.; Giebeler, L.; Rümmeli, M. H.; Eckert, J.; Eychmüller, A.; Kaskel, S. *Advanced Energy Materials* **2014,** 4, (2), n/a-n/a.
12. Wu, H. B.; Wei, S.; Zhang, L.; Xu, R.; Hng, H. H.; Lou, X. W. *Chemistry – A European Journal* **2013,** 19, (33), 10804-10808.
13. Ding, B.; Yuan, C.; Shen, L.; Xu, G.; Nie, P.; Zhang, X. *Chemistry – A European Journal* **2013,** 19, (3), 1013-1019.
14. Zhou, G.; Yin, L.-C.; Wang, D.-W.; Li, L.; Pei, S.; Gentle, I. R.; Li, F.; Cheng, H.-M. *ACS Nano* **2013,** 7, (6), 5367-5375.
15. Lu, S.; Cheng, Y.; Wu, X.; Liu, J. *Nano Letters* **2013,** 13, (6), 2485-2489.
16. Zheng, G.; Zhang, Q.; Cha, J. J.; Yang, Y.; Li, W.; Seh, Z. W.; Cui, Y. *Nano Letters* **2013,** 13, (3), 1265-1270.
17. Zu, C.; Manthiram, A. *Advanced Energy Materials* **2013,** 3, (8), 1008-1012.
18. Su, Y.-S.; Manthiram, A. *Chemical Communications* **2012,** 48, (70), 8817-8819.
19. Zhou, G.; Pei, S.; Li, L.; Wang, D.-W.; Wang, S.; Huang, K.; Yin, L.-

C.; Li, F.; Cheng, H.-M. *Advanced Materials* **2014**, 26, (4), 625-631.
20. Zhang, Y. Z.; Liu, S.; Li, G. C.; Li, G. R.; Gao, X. P. *Journal of Materials Chemistry A* **2014,** 2, (13), 4652-4659.
21. Kinoshita, S.; Okuda, K.; Machida, N.; Naito, M.; Sigematsu, T. *Solid State Ionics* **2014,** 256, (0), 97-102.
22. Song, M.-K.; Zhang, Y.; Cairns, E. J. *Nano Letters* **2013,** 13, (12), 5891-5899.
23. Xu, T.; Song, J.; Gordin, M. L.; Sohn, H.; Yu, Z.; Chen, S.; Wang, D. *ACS Appl Mater Interfaces* **2013,** 5, (21), 11355-62.
24. Li, N.; Zheng, M.; Lu, H.; Hu, Z.; Shen, C.; Chang, X.; Ji, G.; Cao, J.; Shi, Y. *Chemical Communications* **2012,** 48, (34), 4106-4108.
25. Su, Y.-S.; Fu, Y.; Manthiram, A. *Physical Chemistry Chemical Physics* **2012,** 14, (42), 14495-14499.
26. Fu, Y.; Su, Y.-S.; Manthiram, A. *ACS Applied Materials & Interfaces* **2012,** 4, (11), 6046-6052.
27. Zhou, G.; Wang, D.-W.; Li, F.; Hou, P.-X.; Yin, L.; Liu, C.; Lu, G. Q.; Gentle, I. R.; Cheng, H.-M. *Energy & Environmental Science* **2012,** 5, (10), 8901-8906.
28. Zhang, Z.; Li, Z.; Hao, F.; Wang, X.; Li, Q.; Qi, Y.; Fan, R.; Yin, L. *Advanced Functional Materials* **2013**, n/a-n/a.
29. Xin, S.; Gu, L.; Zhao, N.-H.; Yin, Y.-X.; Zhou, L.-J.; Guo, Y.-G.; Wan, L.-J. *Journal of the American Chemical Society* **2012,** 134, (45), 18510-18513.
30. He, G.; Ji, X.; Nazar, L. *Energy & Environmental Science* **2011,** 4, (8), 2878-2883.
31. Sun, F.; Wang, J.; Chen, H.; Qiao, W.; Ling, L.; Long, D. *Scientific Reports* **2013,** 3.
32. Jin, K.; Zhou, X.; Zhang, L.; Xin, X.; Wang, G.; Liu, Z. *The Journal of Physical Chemistry C* **2013,** 117, (41), 21112-21119.
33. Li, G.-C.; Li, G.-R.; Ye, S.-H.; Gao, X.-P. *Advanced Energy Materials* **2012,** 2, (10), 1238-1245.
34. Shin, E.; Kim, M.-S.; Cho, W.; Oh, S. *Nanoscale Research Letters* **2013,** 8, (1), 343.
35. Wang, D.; Yu, Y.; Zhou, W.; Chen, H.; DiSalvo, F. J.; Muller, D. A.; Abruna, H. D. *Physical Chemistry Chemical Physics* **2013,** 15, (23), 9051-9057.
36. Pantea, D.; Darmstadt, H.; Kaliaguine, S.; Roy, C. *Applied Surface Science* **2003,** 217, (1–4), 181-193.
37. Pei, S.; Cheng, H.-M. *Carbon* **2012,** 50, (9), 3210-3228.
38. Park, S.; An, J.; Potts, J. R.; Velamakanni, A.; Murali, S.; Ruoff, R. S. *Carbon* **2011,** 49, (9), 3019-3023.
39. Bhushan, B., *Nanotechnology Handbook*. Springer-Verlag: 2010, p. 47

40. Sánchez-González, J.; Stoeckli, F.; Centeno, T. A. *Journal of Electroanalytical Chemistry* **2011,** 657, (1–2), 176-180.
41. Hurd, J. A.; Vaidhyanathan, R.; Thangadurai, V.; Ratcliffe, C. I.; Moudrakovski, I. L.; Shimizu, G. K. H. *Nature Chemistry* **2009,** 1, (9), 705-710.
42. Marega, R.; Accorsi, G.; Meneghetti, M.; Parisini, A.; Prato, M.; Bonifazi, D. *Carbon* **2009,** 47, (3), 675-682.
43. Kwon, S.; Vidic, R. D. *Environmental Engineering Science* **2000,** 17, (6), 303-313.
44. Yang, S. J.; Cho, J. H.; Nahm, K. S.; Park, C. R. *International Journal of Hydrogen Energy* **2010,** 35, (23), 13062-13067.
45. Zhao, X.; Kim, D.-S.; Ahn, H.-J.; Kim, K.-W.; Cho, K.-K.; Ahn, J.-H. *Materials Research Bulletin,* in press.

국 문 초 록

높은 충방전속도에서도 우수한 성능을 구현하는 리튬황전지를 제조하기 위하여, 다중벽 탄소나노튜브의 벽을 부분적으로 펼침으로써 비표면적, 기공의 총부피 및 폴리설파이드(polysulfide)와 리튬설파이드(lithium sulfide)와 상호작용이 가능한 작용기의 표면개질을 동시에 도모하였다. 그 수단으로써 익숙하고 저렴하며 대량생산화할 수 있는 KOH 활성화를 활용하였으며, 처리시간을 1시간, 2시간, 3시간, 6시간으로 변화시켰다. KOH 활성화를 통해서 다중벽 탄소나노튜브의 벽이 부분적으로 열려져 비표면적과 기공의 부피가 크게 향상된 다공성의 다중벽 탄소나노튜브(porous carbon nanotubes)의 합성을 가능케 하였고, 처리시간에 따라 변화된 형태학적 특성과 표면화학적인 특성이 전기화학적 성능에 미치는 영향을 분석하였다.

또한 부분적으로 펼쳐진 다중벽 탄소나노튜브에 분포된 황의 균일한 정도가 전기화학적인 성능에 미치는 영향을 살펴보았다. 황을 균일하게 분포시키기 위한 방법들 중 대표적인 세가지를 활용하여 다중벽 탄소나노튜브-황 복합체를 준비하여 분석을 진행하였고, 그 결과 용액 기반의 침전반응과 열처리를 함께 도모한 방법이 가장 균일하게 황이 탄소나노튜브 위에 분포시켰으며, 전기화학적인 특성 또한 가장 우수하게 나타났다.

준비된 다공성의 다중벽 탄소나노튜브들 중에 2시간 처리한 것이 가장 우수한 성능을 보여주었다. 빠른 충방전속도인 5 C에서 688 mAh/g의 용량을 나타내었으며, 50회의 충방전이 반복된 뒤에도 672 mAh/g의 높은 용량을 보여주었으며, 우수한 고율특성 뿐만 아니라, 우수한 용량 유지율 또한 나타내었다. 이러한 성능은 비표면적의 증가에 따른 전자의 침투깊이(electron penetration depth)의 감소 효과와 기공의 증가 및 표면에 도입된 작용기에 따른 리튬이온의 확산공간의 보장에 따른 것으로 분석되었다.

주요어 : 다공성 탄소나노튜브, 탄소나노튜브, 리튬황전지, 고율특성, 고성능배터리, 양극 물질.

학 번 : 2012-23151